

# A Novel Water Running Robot Inspired by Basilisk Lizards

Steven Floyd, Terence Keegan, John Palmisano, and Metin Sitti

NanoRobotics Laboratory, Department of Mechanical Engineering, Carnegie Mellon University, PA 15213, USA

**Abstract**—This paper introduces a novel robot which can run on the surface of water in a manner similar to basilisk lizards. Previous studies on the lizards themselves have characterized their method of propulsion and their means of staying afloat. By slapping and stroking their feet into the water, the lizard effects a momentum transfer which provides both forward thrust and lift. The design of a biomimetic robot utilizing similar principles is discussed, modeled, and prototyped. Functionally, the robot uses a pair of identical four bar mechanisms, with a  $180^\circ$  phase shift to achieve bipedal locomotion on the water’s surface. Computational and experimental results are presented and reviewed with the focus being a maximization of the lift to power ratio. After optimization, two legged models can experimentally provide 12-15 g/W of lift while four legged models can provide 50 g/W of lift. This work opens the door for bipedal and quadrupedal robots to become ambulatory over both land and water, and represents a first step toward studies in amphibious stride patterns; step motions equally conducive to propulsion on water and land.

**Index Terms**—Biomimetics, legged robots, basilisk lizard, walking on water.

## I. INTRODUCTION

Small, lightweight animals have a large variety of floatation mechanisms open to them. There are spiders and insects which float using surface tension, and propel themselves using meniscus in the water and marangoni flows. Larger animals have fewer options. Lizards, aquatic birds, and marine mammals, with their larger bulk and higher mass, utilize buoyancy, viscous drag and momentum transfer [1].

The basilisk lizard (*Basiliscus* sp.) is capable of running across the surface of water at approximately 1.5 m/s, and a stepping rate of 5-10 Hz (per leg). Four factors influence the lizard’s ability to stay afloat: a) body mass, b) characteristic length, c) running speed, and d) shape of the foot. All of these variables are inter-related, and the morphological relations to the lizard’s water running have been characterized in [2]–[4], [6], [7].

Biomimetic robots are those machines which emulate some aspect of a living system. In this case, the ability to run over water is what our robot attempts to duplicate. This robot employs momentum transfer for both lift and propulsion, instead of surface tension, which other water walking robots employ [8], [9]. The goal is not to copy nature, but to understand the principles of operation, and use or improve on them for use in our own creations.

The knowledge gained by this work will help expand the limits of legged robot locomotion. A legged robot capable of

walking across land and water quite literally has the entire world open to it. Further work in this field can lead to completely amphibious bipedal or quadrupedal motion. Applications include exploration and search and rescue in partially flooded or marsh-like environments, and of remote controlled toy models which can run anywhere. This work can also help increase the understanding of the basilisk lizard and its ability to walk on both land and water.

In this paper, we use the work of others to develop an understanding of basilisk water running. We then adapt this knowledge to a general four bar mechanism interacting with water to create a computer model with real, predictive value. We first emulate, and then optimize the stepping path of a basilisk lizard. To establish our model’s validity, we built several prototypes, and measured their ability to lift weight out of the water. Lastly, we found ways to improve on nature, and provide our devices with more lifting ability with lower power expenditure.

## II. LIZARD WATER RUNNING

A basilisk’s water running stride can be roughly divided into four phases: slap, stroke, recovery up and recovery down [4]. The forces experienced by the leg and foot are different in each phase, and have differing effects on the lizard’s ability to stay afloat. These phases are shown in Fig. 1. Surface tension effects on the ability to run on the water’s surface are negligible.

### A. Slap Phase

During each step on the water, an initial slap at the interface pushes up on the basilisk’s foot. For younger, lighter lizards, this slap force can provide all of the lift necessary to stay afloat. The lizard’s ability to generate excess lift during the slap phase of the stroke declines as the mass of the lizard increases [3].

The slap phase begins when the foot first contacts the water. Foot motion is primarily downward, and the magnitude of the upward force is much greater than anywhere else in the step. From [3], the maximum slap impulse ( $I_{slap}^{max}$ ) is a function of the effective radius of the foot ( $r_{eff}$ ) and the peak velocity during the slap ( $u_{peak}$ ):

$$I_{slap}^{max} = \frac{4}{3} r_{eff}^3 u_{peak} \quad (1)$$

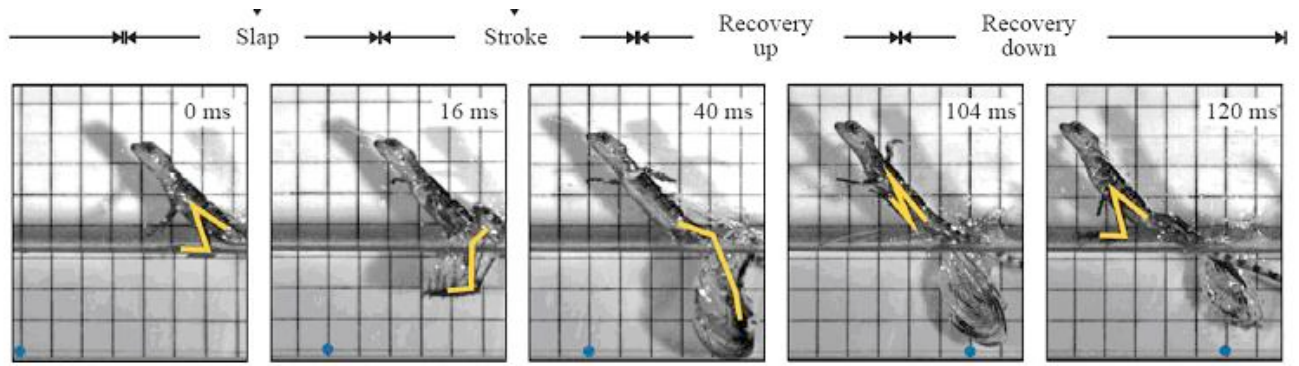


Fig. 1. Phases of a basilisk lizard's step. Time for each frame is shown in milliseconds in the upper right corner. Reprinted with permission from [4].

### B. Stroke Phase

After the slap phase, the lizard pushes against the water beneath its foot, stroking downward and creating an air cavity in the water. The momentum transfer from the lizard's foot to the water during this stroke phase generates the rest of the lift force necessary to stay afloat most of the forward thrust. While basilisk lizards do apply significant forces to the water in a lateral fashion, it is felt this is done for balance and stabilization, and not for lift. Or, this lateral motion may be an anatomical limitation imposed by the creature's posture [6]. It is important for the lizard to retract its foot from the air cavity before it collapses, or it will sink.

For heavier lizards, most of the lift comes from the stroke phase. The drag on the foot is a combination of hydrostatic drag due to increasing depth, and inertial drag from momentum transferred to the fluid. From [2], [3], a good fit for a lizard's foot - or a disk - entering the water is:

$$D(t) = C_D^*[0.5S\rho u^2 + S\rho gh(t)] \quad (2)$$

where  $D(t)$  is the time varying drag force,  $C_D^* \approx 0.703$  is the constant drag coefficient,  $\rho$  is the density of water,  $g$  is acceleration due to gravity,  $S = \pi r_{eff}^2$  is the area over which drag is occurring, and  $h(t)$  is the time varying depth of the foot. This holds true over a large range of velocities for both lizards and experimental equipment.

### C. Recovery Up and Recovery Down

When pulling its foot out of the water during the recovery up phase, the basilisk lizard will curl the toes inward, to prevent accidental drag on the cavity walls. This takes place entirely within the air cavity, and must be completed before the cavity collapses. During recovery down, the speed of the stride increases as the lizard prepares to slap the water surface in the next stride. No significant forces are experienced by the lizard's foot in either of these phases.

### D. Timing

The period of time that the cavity is open ( $T_{seal}$ ) is dependent upon the shape of the foot of the lizard [3]. For a circular disk, the relationship is as follows:

$$T_{seal} = 2.285(r_{eff}/g)^{0.5} \quad (3)$$

This period sets an absolute minimum on the frequency. The lizard must slap down, stroke, and remove its foot from the cavity in less than  $T_{seal}$  seconds. This equation demonstrates that larger feet can, in theory, lead to slower stride frequencies, but there seems to be no correlation in the wild; all basilisks run at the same pace [3].

## III. FOUR BAR MECHANISM MODELING

To mimic the motion of a basilisk's legs, a four bar mechanism in a Grashof crank-rocker configuration was used. Because the four bar mechanism is planar, only the side projection of the lizard's motion can be emulated. After development, the computer model was used to make predictions of the lift a given four bar mechanism could provide.

### A. Kinematics

Fig. 2 shows a four bar linkage and its resultant loop shape. Link A is assumed to be the body, and is considered stationary in all computer models. Lengths of all four linkages are variables, and the angle of Link A is also variable. The tip of Link E is considered the ankle of the mechanism.

Using equations and relations found in [5], it is possible to derive the position and angles of Links C and D given the

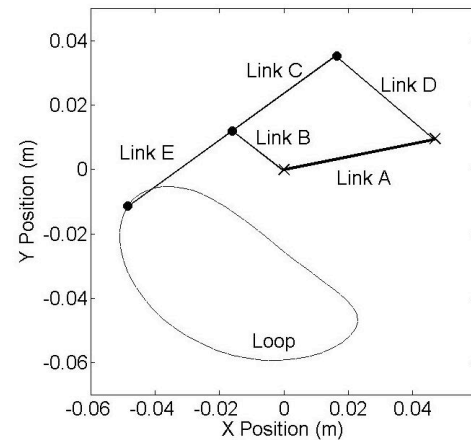


Fig. 2. Diagram of a generic four bar mechanism with links labeled. The loop followed by the tip of Link E is shown.

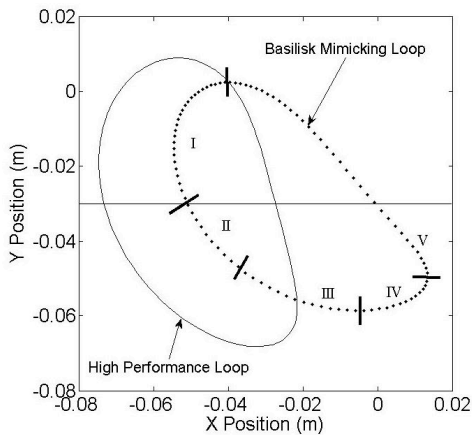


Fig. 3. Two four bar loops. The right loop resembles the step pattern of a basilisk lizard and has the phases of a step marked. I: Recovery Down. II: Slap. III: Stroke. IV: Final push. V: Recovery up. The left loop is a result of iterative improvement, and has a higher performance than the lizard loop.

orientations of Links A and B. Link B is the input link - driven by a motor - and is given a constant angular velocity.

At any given set of angles, one can sum up forces and moments and relate them to the position, velocity, and acceleration of each link. Adding in the external drag forces acting upon the *ankle*, a  $9 \times 10$  matrix can be created to solve for the internal forces on each pin and the input torque applied to Link B. This information can then be used to determine forward thrust and upward lift on a robot as well as the torque required by the motor in order to maintain this motion. All of these forces are functions of position, and must be solved at each orientation discretely. Two hundred positions per revolution are consistently solved for in all simulated results in this paper.

To relate the forces on the ankle,  $F_x$  and  $F_y$ , the relations derived in [2], [3], and presented in Section II are used. The exact conditions used for each phase of a step are described below. Fig. 3 shows an arbitrary step trajectory, with each phase marked.

#### B. Recovery Up and Recovery Down

In the recovery up phase, the foot, though submerged, is assumed to exit the water through the cavity which was formed during the slap and stroke phases. The drag on the foot is thus considered zero. Consequently, both  $F_x$  and  $F_y$  are zero. This phase is characterized in the model as all positions where the ankle velocity vector is upward and toward the left. During the recovery down phase of a step, the foot is above the water level, and is entirely in air, so forces are assumed zero. In the model, this phase lasts for all positions where the ankle height is greater than the water height.

#### C. Final Push

This phase of the step is actually a subsection of the stroke phase, but has different mathematical conditions than the rest of the stroke. It is characterized by the ankle velocity vector being upward and toward the right. During this part of the stroke, it is assumed that only the  $x$ -component of drag exists.

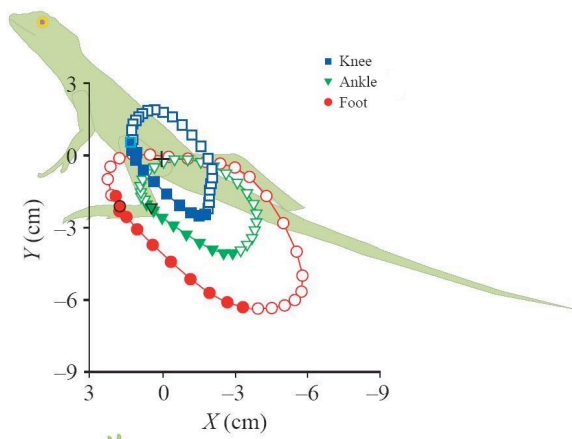


Fig. 4. Lateral view of lizard limb positions relative to its hip. The path of each point is counterclockwise. Solid points indicate stance phase, open points indicate recovery phase. Reprinted with permission from [4]

Because the ankle is rising, and the foot is roughly vertical, any  $y$ -component of drag would be a shear force on the foot, and not a pressure-difference force. Hence, it is assumed the  $y$ -component is negligible, and only the  $x$ -velocity and  $x$ -component of drag are non-trivial. The magnitude of the drag force is given by (2), with the velocity being only the velocity in  $x$ .

#### D. Stroke

In the computer model, the stroke phase begins when the ankle velocity angle is equal to or greater than negative  $45^\circ$ . When this occurs depends on the water height and the loop shape, but in general occurs shortly after the ankle has been submerged. This phase continues until the ankle has reached the lowest point of the loop. Drag on the foot is assumed to be defined by (2), with both  $x$  and  $y$  components of force existing.

#### E. Slap

During the basilisk's step, the slap phase can convey an extra amount of lift, depending upon the speed of contact and the power abilities of the lizard. This phase of the step is for all positions where the ankle height is lower than the water height, and the velocity angle is less than negative 45 degrees. At this time, the slap phase in our simulation is governed by the same equations as the stroke phase. It is hoped that this will yield a conservative estimate on the lift provided by the robot, as the slap phase - in reality - provides a surplus of lift [1]. Future iterations of this model could include a slap phase correction.

#### F. Loop Shaping

With each of the five linkage lengths and the angle of Link A all as variables, initial loop designs were trial and error. It was desired to generate a loop that approximately resembled the path followed by the basilisk during a step. Using charts and figures from [2], the values of each of the link lengths were

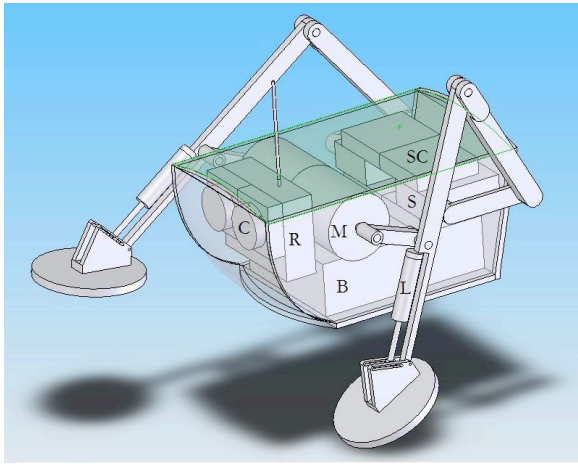


Fig. 5. A CAD rendition of a future version: a fully autonomous, amphibious, water running robot. 2 cameras (C), 1 transmitter/ receiver (R), 2 DC motors (M), 4 speed controllers (SC), 2 servo motors (S), and 2 linear actuators (L) are all powered by a large battery (B). These actuators allow for dynamically changing the foot orientation, the length and orientation of Link A, and the stride speed on each side, which lets the robot optimize its gait and speed for land or water running. The cameras allow for stereoscopic vision, and the ability to estimate the distance to land/water interfaces.

adjusted until they resembled the basilisk stride, as shown in Fig. 3 and Fig. 4.

After the initial shaping, each of the link lengths was varied by a small amount to see the effect on lift. A generic variable called *performance* ( $Pe$ ) was defined, and link lengths were adjusted to maximize it.

$$Pe = \frac{M(g)}{P(W)} \quad (4)$$

$$P = T_{max}(2\pi f) \quad (5)$$

where  $M$  is the mass a loop can lift,  $P$  is the power required to run the loop,  $T_{max}$  is the maximum torque required by the motor, and  $f$  is the step frequency (per leg). As each link length was varied, the performance of the loop was estimated, and compared to the starting point. In this fashion, a crude optimization was iteratively performed, with each successive iteration having a higher performance. This process continued until singularities in the loop started appearing. For all of these optimization steps, it was assumed that the body had an angle of zero; hence, the shafts of Links B and D are at the same height. An improved loop with higher performance than the basilisk mimicking loop was found, and is also shown in Fig. 3.

#### IV. SIMULATIONS

Simulation refinement was occurring simultaneous to experiments, with both methods being used to improve each other. Because many simulations could be performed in a short amount of time, it was used to predict the effect of altering design parameters before experimenting. Experiments were then performed to confirm simulated results, and improve the computer model. Once the computer model was giving approximate results (within 50%), and was responding to variable changes in a manner similar to reality, it was used to optimize several geometric relations.

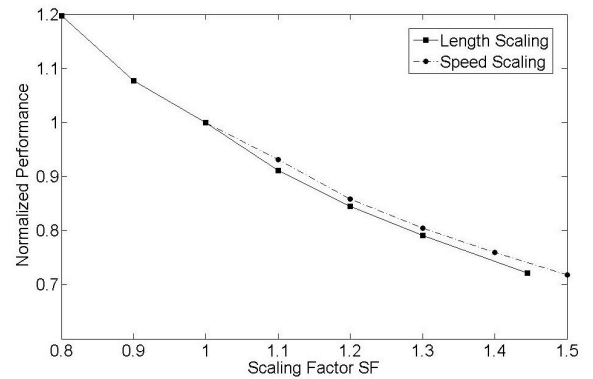


Fig. 6. Simulated effects of characteristic length and speed scaling on a four bar mechanism with link lengths A=48, B=16, C=55, D=30, E=40 (mm).

The results of varying several different parameters are discussed. For these tests, the height of the water was assumed to be at the time averaged  $y$ -location of the loop, so that 50% of the time is spent above and 50% of time is spent below the water line. A computer aided design (CAD) model of a possible future robot is presented in Fig. 5, and serves as a visual representation of the system being modeled.

##### A. Length and Speed Scaling

To increase the lift that a four bar mechanism provides, one can maintain the relative link lengths, and simply multiply them all by a scaling factor,  $SF$ . We wished to know if the performance of a given loop could be improved by scaling upwards or downwards, or if an optimum size scale existed.

Another method to increase lift is to increase the stepping frequency. From (3), there is a minimum velocity that must be maintained for the foot to escape the cavity collapse. This is based almost entirely on the effective radius of the foot, and for different four bar linkages with the same foot diameter, this lower limit is a constant. Hence, for speed scaling  $SF \geq 1$ . Once again, we wished to know if there was an optimum speed, a general trend, or no effect on performance.

The results of scaling link lengths and speed are shown in Fig. 6. Results are normalized so that when the  $SF = 1$ ,  $Pe = 1$ . One can see that as the length scale increases, the performance decreases. Hence, smaller length scales have higher performance. Speed, like length, also scales negatively. Slower speeds approaching the cavity collapse limit have the highest performance. The exact relationship of each is dependent upon the loop itself, and bears no immediate physical meaning.

Between the two, it seems that speed scaling is slightly preferable. Hence, if the lift ability of a given loop must be increased, it is better to increase speed than to increase length.

##### B. Foot Diameter

A third method to increase the lift capacity of a four bar mechanism is to increase the diameter of the foot. This has two effects: larger diameters lead to larger  $T_{seal}$  from (3), and hence lower stride frequency, and the larger area leads to larger drag forces from (2). Lower stride frequencies lead to higher

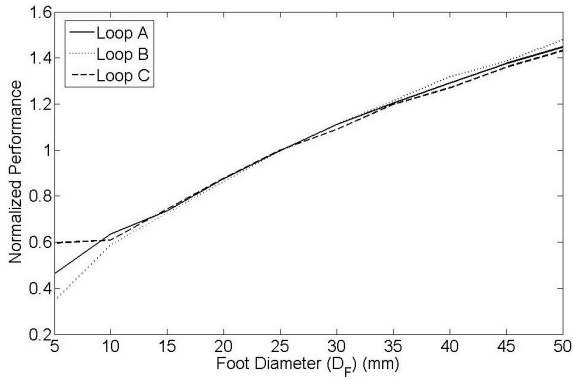


Fig. 7. Simulated effect of adjusting the foot diameter. Loop A: link lengths A=40, B=16, C=40, D=24, E=32 (mm). Loop B: link lengths A=48, B=16, C=55, D=30, E=40 (mm). Loop C: link lengths A=50, B=20, C=40, D=40, E=40 (mm).

performance, as seen in Fig. 6, but larger drag forces will increase both the lift and power requirements. As in the speed and length scaling cases, we wished to know if there was an optimum foot diameter, a trend, or no effect on performance.

Fig. 7 shows that as the foot diameter is increased, the performance also increases. Further, this effect seems to be independent of loop shape, as demonstrated by the similarity of the normalized performance lines for all three four bar linkages. The performance scales with  $D_F^{0.5}$ , which is logical. Examination of (2), (3) and (4), combined with the knowledge that power scales with force multiplied by speed, one can see the numerator of (4) scales with  $D_F^2$ , and the denominator scales with  $(D_F^2)(D_F^{-0.5})$ . Hence, to maximize performance, increase the foot diameter. The limitations of the diameter are placed by practical, and not theoretical constraints; determine the largest foot diameter for a robot that is reasonable in relation to the rest of the body. In our experiments,  $D_F = 40$  (mm) for all trials.

### C. Foot Angle

When the basilisk runs on water, it adjusts its foot angle throughout the step. This maximizes the lift and thrust generated, and also allows the lizard to streamline its foot during the recovery phase. For this simple device, a static foot angle is most easily achieved when using rigid, passive components.

For initial predictions, it was assumed the foot angle would be ideal throughout the loop; i.e. that the plane of the foot would be perpendicular to the velocity vector direction. This is not possible with a non-dynamic foot, so the program was adjusted to incorporate a set foot angle. The angle was then varied to determine the optimum. Zero degrees was assumed to be in line with Link C, and angles follow the counterclockwise convention.

The results of these tests are shown in Fig. 8. This is another loop dependent optimization, so these tests were performed on the highest performing loop from the iteration stages. For angles between  $-5^\circ$  and  $10^\circ$ , there is only a slight decrease in the lift provided. To ease assembly of prototypes, all tests were done with  $0^\circ$  foot angle.

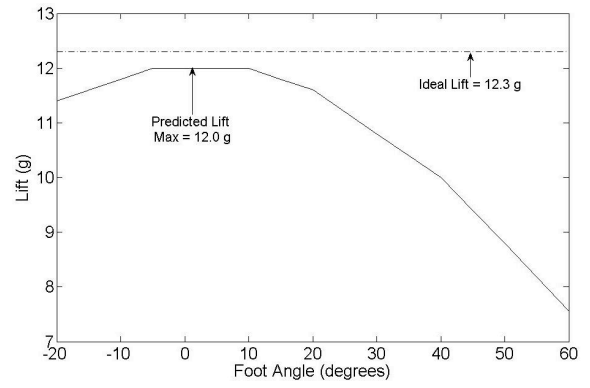


Fig. 8. Simulated effect of adjusting the foot angle. Done for link lengths A=48, B=16, C=55, D=30, E=40 (mm).

For these tests, performance is not a useful metric because it remains nearly unchanged for each foot angle. This is logical because foot angles which provide less lift require less power to move the foot through the step path.

### D. Extra Legs

Throughout the simulated results, power required was taken as the maximum torque multiplied by the speed. But, the torque required throughout each step varies greatly and, depending on the loop, can even drop below zero. If an extra pair of legs is added, phase shifted by  $90^\circ$  from the first pair, then it might be possible to double the lift while only marginally increasing the power requirements. Similar scaling will also occur if 4 more legs are added to that. The effect to the torque can be seen in Fig. 9.

After 8 legs, one enters the realm of diminishing returns when it comes to increasing performance. For the link lengths A=48, B=16, C=55, D=30, E=40 (mm), two legs yields a performance of 32 g/W, and four legs yields 55 g/W, but eight legs only lifts 58 g/W. But, it is interesting to note that increasing the number of legs beyond eight can increase the lift while maintaining the same performance. This implies that the best way to boost lift is to increase the number of legs, not scale the length or the speed. Effectively, one can decouple the speed effects from the lift entirely, and use a speed control for both turning and stability.

## V. EXPERIMENTS

To test the simulation results, a two-legged setup, similar to Fig. 10, was created. This was supported with carbon fiber - and later, acrylic - struts connected to a counter weight. Both the mass of the test robot and the counter weight mass were above the fulcrum height; hence, the system was unstable, and tended to fall one way or the other. On the robot side, there was a support under the struts, allowing the robot to rest at a slight angle with the counter weight suspended in the air. The fulcrum of this counterweighted system was placed as close as possible to a central shaft, about which the entire assembly could revolve during testing. A ten pound weight held the central shaft and assembly in place in a tub of water during testing.

### A. Testing Procedure

First, the height of the input axle was measured relative to the tub bottom as a reference point. Water was added to the tub until the feet of the robot could interact with it (approximately 2-3 mm above the lowest point of the toe path) and the height was measured relative to the axle height. Then, the counter weight was moved to the point where the two bodies were perfectly balanced with the struts are exactly horizontal. The motor was started, and the robot was lightly held down until transient vibrations diminished. After letting go, if the robot pushed itself up and over the stable point, weight was added to the robot until it could no longer push itself up. Afterward, the system was rechecked to ensure it was still in its balanced position (which shifts as the machine gets wet). The weight was recorded, more water was added, and the procedure was repeated.

To ensure that the vibrations of the motor itself did not cause the robot to push over its stable point, each four bar system was run after calibration while dry. This led to a large spacing between the fulcrum and the robot system, and a large amount of upward push required to lift it. On later trials, when excessive vibration *did* excite the machine over its stable point, the struts were remade and mild damping was added.

### B. DC Motor Results

Initially, a DC motor was used to test simulated predictions and refine the computer model. Testing was performed for various loop configurations, to determine if the computer accurately predicted more optimized loops. This motor had no speed control, so the speed used in predicting lift was the in-air motor speed, approximately 5 Hz, determined using a stroboscope. Results are shown in Fig. 11.

Because DC motors were used, the speed decreased as torque increased. These results showed that, while overestimating, the predictor program had a slope similar to reality, and could take into account varying water levels accurately. This led to improvement of the estimator for later trials.

### C. Stepper Motor Results

More promising and accurate results were found when a stepper motor was used. Because speed can be controlled with

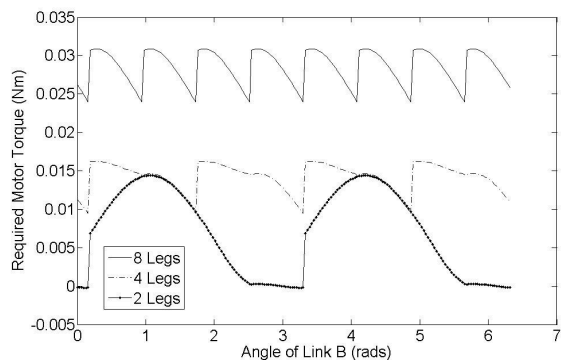


Fig. 9. Simulated torque throughout a single revolution for 2, 4, and 8 legs. Done for Link A=40, Link B=16, Link C=40, Link D=24, Link E=32 (mm).

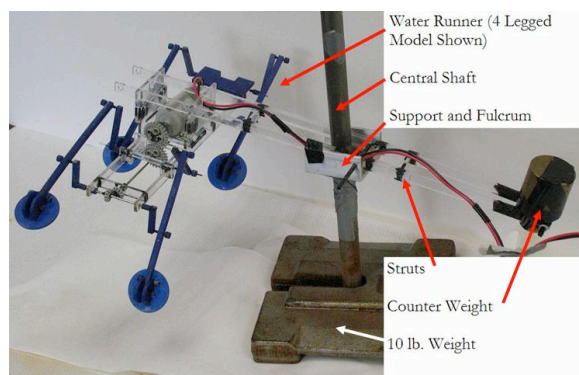


Fig. 10. Photo of the four legged experimental setup used for testing. Two legged versions with variable link lengths were also used to test the accuracy of the computer models.

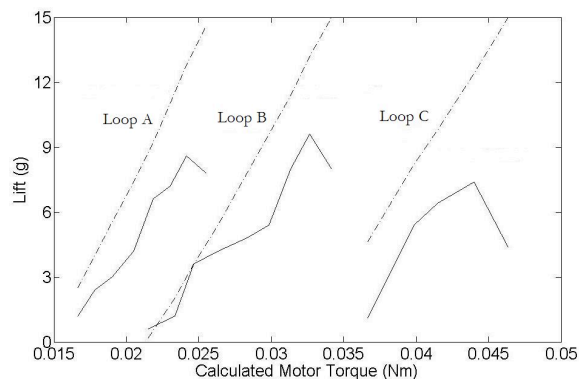


Fig. 11. Experimental DC motor results for three 4 bar sets. Dash-dot lines are theoretical predictions; regular lines are experimental data. Loop A: link lengths A=40, B=16, C=40, D=24, E=32 (mm). Loop B: link lengths A=40, B=16, C=32, D=32, E=32 (mm). Loop C: link lengths A=40, B=16, C=24, D=40, E=40 (mm). All tests were run at 5 Hz.

a stepper motor, more accurate information could be provided to the estimator program. One can see from Fig. 12 that the results of experiment and theory more closely match, and the maximum lift we are getting is 17 grams at 6 Hz. For this result  $P_e = 15 \text{ g/W}$ . These results are still much lower than the lift a basilisk lizard can generate, around 34 g/W [7]. These experiments were carried out on a high performance loop while varying the motor speed.

### D. Four Legged Results

As mentioned in Section IV, simulation results implied four legs would have a higher performance than two legs. As such, the experimental setup shown in Fig. 10 was used. This was once again driven by a DC motor without speed control, because of the higher power ratings and the ease of installation. Using a scaled up version of a high performance loop, the front and back legs are driven at the same speed, offset by  $90^\circ$ . The results of testing are shown in Fig. 13.

The four legged results are, in appearance, similar to the two legged DC motor results. This implies that if a powerful, speed controlled motor is used, the lift curve should resemble the two legged stepper motor results, in Fig. 12, and the theoretical and experimental lifts would converge. The maximum lift provided

was 16.6 g, which results in  $Pe = 49.5$  g/W, greater than what two legged basilisk lizards produce.

## VI. CONCLUSIONS AND FUTURE WORK

In this paper, a robotic propulsion system based upon the water running ability of basilisk lizards is modeled and tested. Using four bar mechanisms as legs, two legged models can lift upwards of 15 g/W. Employing equations of motion found in the literature, a computer model with predictive value is developed, and is used to optimize the physical design. From these simulations and optimizations, four legged versions are found to have superior performance compared with two legged robots. Four legged robots can provide upwards of 50 g/W, an increase of over 200%. The effects of altering several design variables, including characteristic length, running frequency, foot angle, and the lengths of each link in the four bar mechanisms are simulated. From this, we determined that both speed and length scale negatively, with lower performance at higher frequencies and longer links. For our highest performing loop, the angle of the foot provides the largest lift when near zero°, relative to Link E. Our mathematical predictions are confirmed through experimentation with both a DC and stepper motor for the two legged model, and a DC motor for the four legged model.

Our future work will be toward creating a device capable of lifting its own weight while water running. In addition to creating enough lift and thrust, we are investigating implementation of a control system and incorporating a steering mechanism. We will be increasing the degrees of freedom in the system, including, but not limited to: actuated ankles, individual leg speed control, and energy storing springs for land locomotion. We are also investigating including additional joints to make each four bar mechanism dynamic, so we can adjust loop shape when transitioning from water to land, much like the device shown in Fig. 5. Our ultimate goal is a fully autonomous and amphibious water runner capable of traversing both land and water.

Some issues that will have to be addressed are those dealing with the interaction of mechanical and electrical components with water. All wiring and exposed electronics must be shielded

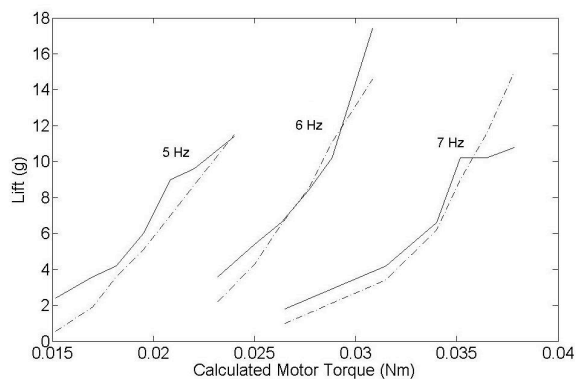


Fig. 12. Experimental stepper motor results for three 4 bar sets. Dash-dot lines are theoretical predictions; regular lines are experimental data. Done for link lengths A=40, B=16, C=40, D=24, E=32 (mm).

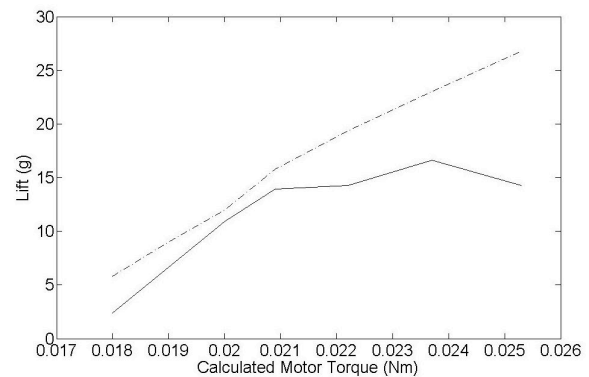


Fig. 13. Experimental DC motor results for a four legged model. Dash-dot lines are theoretical predictions; regular lines are experimental data. Done for link lengths A=65.3, B=21.8, C=74.8, D=40.8, E=54.4 (mm).

from the water for safety purposes and to prevent harmful shorts from damaging any of the systems. Mechanical parts must be rust proof and, preferably would be either hydrophobic, or have a hydrophobic surface treatment. This would prevent loss of lift to the accumulation of water on the robot's surface. Also, actuators and power sources must be chosen to be light weight yet highly efficient to reach the performance anticipated by simulations. Lastly, light weight, high strength materials must be chosen for the legs to minimize torque required to move them through space, and to keep the mass distribution as central as possible.

## ACKNOWLEDGMENT

The authors would like to thank S. Tonia Hsieh for allowing us to reprint her figures, and Mike Murphy for all his help with the rapid prototyping machine.

## REFERENCES

- [1] J. Bush and D. Hu, "Walking on Water: Biocomotion at the Interface," *Annu. Rev. of Fluid Mech.*, 38, pp. 339-369, 2006.
- [2] J. Glasheen and T. McMahon, "Vertical water entry of disks at low Froude number," *Phys. Of Fluids*, 8, pp. 2078-2083, 1996.
- [3] J. Glasheen and T. McMahon, "Size-Dependence of Water-Running Ability in Basilisk Lizards (*Basiliscus Basiliscus*)," *The Journal of Experimental Biology*, 199, pp. 2611-2618, 1996.
- [4] S. Hsieh, "Three-dimensional hind limb kinematics of water running in the plumed basilisk lizard (*Basiliscus plumifrons*)," *The Journal of Experimental Biology*, 206, pp. 4363-4377, 2003.
- [5] <http://iel.ucdavis.edu/chhtml/toolkit/mechanism>
- [6] T. Hsieh and G. Lauder, "Running on water: Three-dimensional force generation by basilisk lizards," *PNAS*, 101, pp. 16784-16788, 2004.
- [7] J. Glasheen and T. McMahon, "A hydrodynamic model of locomotion in the Basilisk Lizard," *Nature*, 380, pp. 340-342, 1996.
- [8] Y. Song, S. Suhr, and M. Sitti, "Modeling of the Supporting Legs for Designing Biomimetic Water Strider Robots," *Proceedings of International Conference on Robotics and Automation (ICRA)*, 2006.
- [9] D. Hu, B. Chan, and J. Bush, "The hydrodynamics of water strider locomotion," *Nature*, 424, pp. 663-666, 2003.